

Cite this: *RSC Adv.*, 2018, 8, 1979

Insight into the synergism between MnO₂ and acid sites over Mn–SiO₂@TiO₂ nano-cups for low-temperature selective catalytic reduction of NO with NH₃†

Siyi Zheng,^a Lei Song,^a Siyang Tang,^a Changjun Liu,^{ab} Hairong Yue^{id}*^a and Bin Liang^{ab}

The rational synthesis of low-temperature catalysts with high catalytic activity and stability is highly desirable for the selective catalytic reduction of NO with NH₃. Here we synthesized a Mn–SiO₂/TiO₂ nano-cup catalyst via the coating of the mesoporous TiO₂ layers on SiO₂ spheres and subsequent inlay of MnO₂ nanoparticles in the narrow annulus. This catalyst exhibited superior catalytic SCR activities and stability for low-temperature selective catalytic reduction of NO with NH₃, with NO conversion of ~100%, N₂ selectivity above 90% at a temperature ~140 °C. The characterization results, such as BET, XRD, H₂-TPR, O₂/NH₃-TPD and XPS, indicated that this nano-cup structure catalyst possesses high concentration and dispersion of Mn⁴⁺ active species, strong chemisorbed O[–] or O₂^{2–} species and highly stable MnO_x active components over the annular structures of the TiO₂ shell and SiO₂ sphere, and thus enhanced the low-temperature SCR performance.

Received 27th October 2017
Accepted 23rd December 2017

DOI: 10.1039/c7ra11868f

rsc.li/rsc-advances

1. Introduction

The combustion of fossil fuels, *i.e.*, coal, petroleum and natural gas in stationary and mobile sources generates massive NO_x emissions in the world, which gives rise to serious environmental problems such as the formation of acid rain, haze, photochemical smog and the depletion of ozone.^{1–6} The selective catalytic reduction (SCR) of NO_x with NH₃ is a crucial methodology for the reduction of NO_x emissions from stationary sources, such as coal-fired power plants, because of its low cost and high efficiency. The current technologies for the industrial SCR processes primarily employ commercial V-based catalysts and operate at temperatures of 300–400 °C.^{7–9} There are some key issues for the high-temperature SCR process, such as obligatory placement of the catalysts in the upstream of the electrostatic precipitator and desulfurizer, catalytic deactivation by SO₂ or fly ash, and the generation of N₂O at high temperature.^{10–13} In addition, the toxicity of V-based catalysts is detrimental to the environment and human-beings. Therefore, the rational design and development of excellent and green catalysts at low temperature is vital for the SCR of NO_x with NH₃.

The transitional metal oxides, including FeO_x, CeO₂, NiO, CuO and MnO_x have been extensively investigated for the SCR reaction at the temperature below 300 °C.^{8,14–16} The MnO_x based catalysts possess excellent low-temperature activity and environmentally benign property, and were regarded as excellent candidates for the industrial application in SCR reaction.^{17–23} The strong redox property of Mn⁴⁺ as the dominant valence species and the low crystallinity of MnO_x nanoparticles in MnO₂ catalysts is crucial to promote the oxidation of NO to NO₂ and lead to an excellent low-temperature NH₃-SCR activity.^{24–27} Pena *et al.* found that the MnO_x catalysts with different valence states and labile oxygen contributed to the excellent SCR performance in a low temperature of 120 °C. The presence of chemisorbed oxygen, which is more active than the lattice oxygen, could also facilitate the oxidation of NO for the formation of nitrates and result in a high NO conversion.^{28–31}

In addition, the catalyst support with Brønsted and/or Lewis acid sites was verified to enhance the adsorption of NH₃ through three hydrogen bonds, and thus facilitate the low-temperature NH₃-SCR reaction. Recently, Boningari *et al.* reported the NH₃-SCR reaction mechanism over Mn-based catalysts via the correlation of activity with the acidity, manganese oxide valence state and morphology.³² The results indicated that the high dispersion of MnO_x and appropriate surface acidity play a synergistic effect on the SCR reaction. TiO₂ is a widely used catalyst support for its stable chemical properties and environmental friendliness, especially the excellent resistance of SO₂ for the SCR reaction in the industrial flue gas.^{12,16,33,34} The

^aMulti-phases Mass Transfer and Reaction Engineering Laboratory, School of Chemical Engineering, Sichuan University, Chengdu 610065, China. E-mail: hryue@scu.edu.cn; Fax: +86 22 85997677; Tel: +86 22 85997677

^bInstitute of New Energy and Low-Carbon Technology, Sichuan University, Chengdu 610207, China

† Electronic supplementary information (ESI) available. See DOI: 10.1039/c7ra11868f

nature of TiO_2 , such as facet, shape and acid sites, also plays an essential role in the catalytic activities and long-term stability.^{35,36} Deng *et al.* reported that $\text{MnO}_x/\text{TiO}_2$ catalyst with a preferentially anatase TiO_2 facet facilitated high NO conversion and low N_2O selectivity at 80–280 °C.³⁷ Zhang *et al.* reported that the fabrication of core-shell nanomaterials could stabilize the active species and enhance stability.³⁸ Therefore, the rational synthesis of TiO_2 supported Mn catalysts with unique morphologies and surface chemistry for the high efficiency and stability is vital for the catalytic SCR reaction.^{24,39–41}

Herein, a novel $\text{Mn-SiO}_2@\text{TiO}_2$ nano-cup catalyst was synthesized *via* the coating of the mesoporous structured anatase TiO_2 layers on the SiO_2 spheres and subsequent inlay of MnO_2 nanoparticles (NPs) in the narrow annulus. The chemical etching method was introduced to tune the structures of TiO_2 layers and the size of SiO_2 nano-spheres, aiming at the fabrication of highly dispersed MnO_2 NPs and appropriate acid sites for SCR reaction. The catalysts were systematically investigated to understand surface chemistry as well as the evolution of structures and active sites. The synergic mechanism between MnO_2 and acid sites over the $\text{TiO}_2@\text{SiO}_2$ support for low-temperature SCR reaction was also proposed on the basis of the experimental results.

2. Experimental section

2.1 Catalysis preparation

Preparation of $\text{SiO}_2/\text{TiO}_2$ nanocups. The formation process of $\text{SiO}_2/\text{TiO}_2$ nano-cup was illustrated in Fig. 1. All reagents, purchased from the Sinopharm Chemical Reagent Co., Ltd (China), were of analytical standard and used without any further purification. Firstly the mixture of tetraethyl orthosilicate (TEOS, 28%, 3.84 mL), deionized water (17.2 mL), dehydrated ethanol (99.8%, 92 mL) and ammonia solution (26%, 2.48 mL) was stirred for 4 h at room temperature. The spherical SiO_2 templates were separated from the mixture by centrifugation and washed with ethanol for 3 times. Then the spherical SiO_2 were dispersed in a mixture of hydroxypropyl cellulose (HPC, 0.4 g), ethanol (80 mL), and deionized water (0.4 mL). After stirring for 40 min, titanium *tert*-butoxide (TBOT, 98%, 4 mL) in 20 mL ethanol was added dropwise into the mixture with stirring under reflux conditions for 100 min until the suspension was heated to 85 °C. The final product was isolated using centrifugation and calcinated in air at 500 °C for 2 h (heating rate of 2 °C min⁻¹). The obtained $\text{SiO}_2@\text{TiO}_2$ samples in 40 mL water were added with 8 mL NaOH (1.25 M) and treated for

several hours (*i.e.*, 1.5, 2.5 and 3 h) to tune the size of SiO_2 and the TiO_2 layers. Then the samples were washed by ethanol for several times and dried at 80 °C for 6 h. The obtained samples were denoted as the $\text{SiO}_2@\text{TiO}_2$, $\text{SiO}_2@\text{TiO}_2$ -1.5, $\text{SiO}_2@\text{TiO}_2$ -2.5 and $\text{SiO}_2@\text{TiO}_2$ -3.

Preparation of $\text{Mn-SiO}_2/\text{TiO}_2$ nano-cup catalysts. The catalysts were prepared by ultrasonic impregnation method using manganese nitrate as the precursor. Firstly, the SiO_2 and $\text{SiO}_2@\text{TiO}_2$ spheres, and $\text{SiO}_2@\text{TiO}_2$ nanocups were dispersed in water with precursor added and stirring for 0.5 h, and then under ultrasonic treatment (25 kHz and 400 W) for 2 h. The mixture was first dried at 110 °C for 12 h and calcined at 250 °C for 3 h, respectively. The amount of Mn loaded on all the catalysts was 15 wt%. The obtained catalysts were denoted as the Mn/SiO_2 , $\text{Mn-SiO}_2@\text{TiO}_2$, $\text{Mn-SiO}_2@\text{TiO}_2$ -1.5, $\text{Mn-SiO}_2@\text{TiO}_2$ -2.5 and $\text{Mn-SiO}_2@\text{TiO}_2$ -3.

2.2 Characterizations

To observe the morphologies and the structures of the samples, the field emission scanning electron microscopy (SEM, JEM-7500F, Japan JEOL) was introduced to obtain the microstructure of the catalysts. The N_2 adsorption isotherm of the catalysts was obtained on ASAP 2460 (Micromeritics, USA) at -197 °C. The specific surface area was calculated based on the standard Brunauer-Emmett-Teller (BET) theory, while the pore volume and pore-size distribution using the Barrett-Joyner-Halenda (BJH) method. The powder X-ray diffraction (XRD) pattern was recorded on a Bruker D8 Advance diffractometer with $\text{CuK}\alpha$ radiation to investigate the crystallographic phase of the samples with a 2θ range of 10–80° and a step size of 0.026°. Inductively coupled plasma (ICP) method was used to determine the chemical composition of catalysts on a Varian Vista Axial instrument. To obtain the chemical states of catalysts elements on their surface, X-ray photoelectron spectroscopy (XPS) measurement was applied on the Thermo Fisher Scientific K-Alpha instrument with monochromatic Al $\text{K}\alpha$ radiation.

The surface acidity of the catalysts was detected using the temperature-programmed desorption of ammonia (NH_3 -TPD) on a Quantachrome Autosorb-IQ-C chemisorption analyser. The sample powders were firstly pre-treated in pure He at 300 °C for 1 h and then cooled down to 80 °C. The catalysts were constantly saturated in anhydrous NH_3 (10% in He) at a flow rate of 30 mL min⁻¹ for 30 min and the physical adsorption of NH_3 was removed by He for 30 min. Finally, the desorption was carried out by heating the samples from 80 to 650 °C at a heat rate of 10 °C min⁻¹. The oxygen temperature-programmed desorption (O_2 -TPD) and H_2 temperature-programmed reduction (H_2 -TPR) were also performed on the Quantachrome Autosorb-IQ-C chemisorption analyser. For the O_2 -TPD experiment, 0.1 g sample was firstly pre-treated in pure He at 250 °C for 30 min and then cooled down to 50 °C. Then the samples were treated under pure oxygen for 1 h and the oxygen desorption was carried out by heating the sample from 50 °C to 750 °C. For H_2 -TPR experiment, 0.05 g of catalyst sample was pre-treated at 200 °C in pure Ar for 1 h and then cooled down to room temperature. Then the tests were conducted under 10% H_2/Ar at

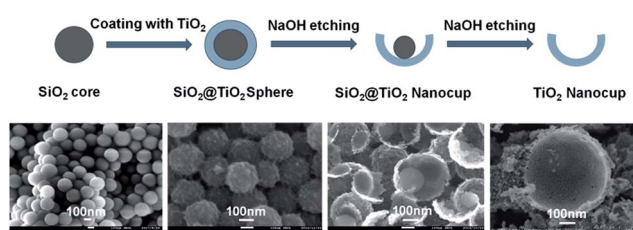


Fig. 1 The formation process of $\text{SiO}_2@\text{TiO}_2$ and TiO_2 nano-cups.



a heat rate of $10\text{ }^{\circ}\text{C min}^{-1}$ from room temperature to $800\text{ }^{\circ}\text{C}$. The signal of H_2 , O_2 and NH_3 was recorded by the thermal conductivity detector (TCD).

2.3 Activity test

The catalytic activity was tested in a fixed-bed stainless steel flow reactor (i.d. = 8 mm) at atmospheric pressure. The reaction conditions were set as follows: 0.21 g of catalyst, 1000 ppm NH_3 , 1000 ppm NO , 5 vol% O_2 , N_2 as the balance, and the total gas flow rate was 200 mL min^{-1} , and the gas hourly space velocity (GHSV) was $30\text{ }000\text{ h}^{-1}$. The concentrations of NO and NO_2 were measured by a Laoying 3022 Flue Gas Analyser, and the N_2O was monitored by a ThermoStar Mass Spectroscopy Analyser.

All activity data was recorded after 60 min when the reaction condition was steady. The NO_x conversion and N_2 selectivity were calculated by:⁴²

$$\text{NO}_x \text{ conversion (\%)} = \frac{[\text{NO}_x]_{\text{in}} - [\text{NO}_x]_{\text{out}}}{[\text{NO}_x]_{\text{in}}} \times 100\% \quad (1)$$

$$\text{N}_2 \text{ selectivity (\%)} = \left(1 - \frac{[\text{N}_2\text{O}]_{\text{out}}}{[\text{NO}_x]_{\text{in}} - [\text{NO}_x]_{\text{out}}}\right) \times 100\% \quad (2)$$

3. Results and discussion

3.1 The formation and the morphologies of the catalysts

The formation of $\text{Mn-SiO}_2@\text{TiO}_2$ nano-cup catalysts involved the preparation of the TiO_2 or $\text{SiO}_2@\text{TiO}_2$ nano-cups and subsequent inlay of MnO_2 NPs in the narrow annulus using ultrasonic impregnation. As shown in Fig. 1, the spherical SiO_2 template was first synthesized *via* the hydrolysis of TEOS, and the TiO_2 shell on the SiO_2 spheres was formed by the hydrolysis of tetrabutyl titanate. The amorphous TiO_2 shell was transformed into the anatase phase in the calcination process at $500\text{ }^{\circ}\text{C}$. Then the $\text{SiO}_2@\text{TiO}_2$ nano-spheres were put into the NaOH solution for different time to partly remove the SiO_2 core and TiO_2 layer. The corresponding SEM images in Fig. 2 showed that the surface of SiO_2 spheres is pretty smooth, while the

surface of $\text{SiO}_2@\text{TiO}_2$ is rather rough, indicating the TiO_2 was perfectly clad around the SiO_2 spheres. After 1.5 h etching treatment with NaOH , the $\text{SiO}_2@\text{TiO}_2$ samples showed small opening holes on the TiO_2 outer layer encapsulated with SiO_2 spheres. The increase of etching time enlarged the opening holes and reduced the inside SiO_2 core as nano-cup structures at 2.5 h. Further increase of the etching time will lead to disappear of inner SiO_2 core at about 3 h. The formed well-defined nanocups are with uniform diameter size of about $300 \pm 10\text{ nm}$. The etched samples possess larger specific surfaces ($93.16\text{ m}^2\text{ g}^{-1}$ at 2.5 h) compared with the no etching $\text{SiO}_2@\text{TiO}_2$ samples ($40.25\text{ m}^2\text{ g}^{-1}$). The large pores and specific surface of the nano-cups could ensure the MnO_2 active species loaded on the support with a high dispersion, and facilitate the adsorption of NH_3 on the surface for the SCR reaction. Therefore, the MnO_2 species were uniformly and well deposited on the surface of the $\text{SiO}_2@\text{TiO}_2$ and TiO_2 nano-cups, and no obvious agglomerates was observed from the SEM images of the MnO_2 loaded samples in Fig. 2.

The physical properties of Mn-based catalysts were listed in Table 1. The results showed a much small surface area for the Mn/SiO_2 ($20.3\text{ m}^2\text{ g}^{-1}$) and $\text{Mn-SiO}_2@\text{TiO}_2$ ($35.9\text{ m}^2\text{ g}^{-1}$) samples, and small pore volume of Mn/SiO_2 catalyst ($0.072\text{ cm}^3\text{ g}^{-1}$). But the $\text{Mn-SiO}_2@\text{TiO}_2$ nano-cup catalysts possessed large BET surface areas, with the largest BET surface of $89.98\text{ m}^2\text{ g}^{-1}$ and pore volume of $0.22\text{ cm}^3\text{ g}^{-1}$ for the $\text{Mn-SiO}_2@\text{TiO}_2$ -2.5 catalyst. The further extension of the etching time led to a decrease of specific surface area. The average pore diameter of all the catalysts is about 10–14 nm. It was suggested that larger surface area and appropriate pore diameter (*e.g.*, $>3\text{ nm}$) were beneficial to the NH_3 adsorption and the SCR performance.⁴³

The XRD patterns of the catalysts were shown in Fig. 3. The diffraction peak of the anatase TiO_2 was detected in all the samples. The increase of the etching time weaken the peaks of anatase TiO_2 , suggesting that the etching treatment could result in a lower crystallinity of TiO_2 layer. In addition, the strong peaks of MnO_2 and Mn_2O_3 were detected in the Mn-SiO_2 , $\text{Mn-SiO}_2@\text{TiO}_2$, $\text{Mn-SiO}_2@\text{TiO}_2$ -1.5 catalysts. While in the $\text{Mn-SiO}_2@\text{TiO}_2$ -2.5 and $\text{Mn-SiO}_2@\text{TiO}_2$ -3 catalysts, the intensities

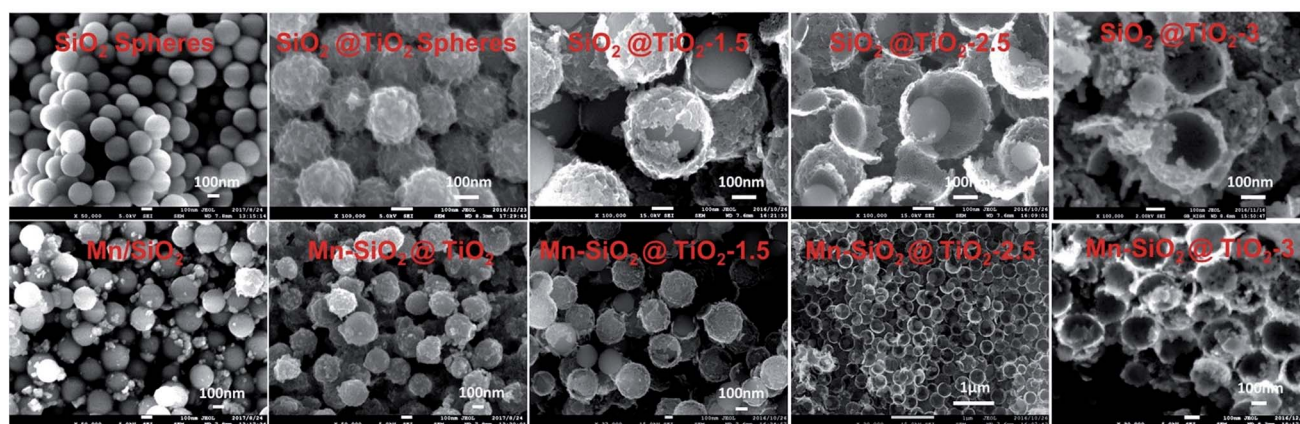


Fig. 2 The SEM images of nano-sphere/nano-cup supports and MnO_2 -based catalysts.



Table 1 The physical properties of the Mn-based nano-cup catalysts

Samples	SSA ^a (m ² g ⁻¹)	Pore volume ^a (cm ³ g ⁻¹)	Pore diameter ^a (nm)	Mn ^b (wt%)	Rate constant ^c
Mn/SiO ₂	20.34	0.072	14.17	13.45%	3.00 × 10 ²
Mn-SiO ₂ @TiO ₂	35.91	0.118	13.18	12.67%	9.83 × 10 ²
Mn-SiO ₂ @TiO ₂ -1.5	69.86	0.190	11.43	13.85%	5.24 × 10 ²
Mn-SiO ₂ @TiO ₂ -2.5	89.98	0.223	10.18	14.76%	1.90 × 10 ³
Mn-SiO ₂ @TiO ₂ -3	77.05	0.214	11.22	14.22%	1.48 × 10 ³

^a Specific surface area (SSA) and pore volume by N₂-adsorption method. ^b Mn content of the catalysts quantified by ICP-OES. ^c Pseudo-first order rate constant at 140 °C.

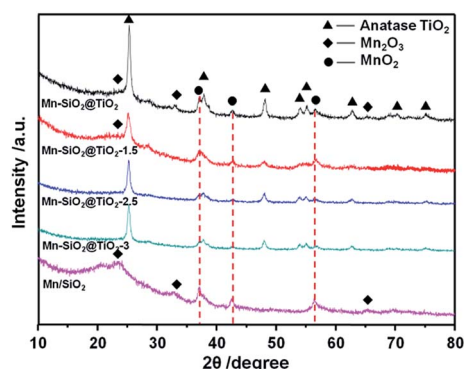


Fig. 3 XRD patterns of the Mn-based nano-cup catalysts.

of MnO₂ were much lower, indicating the highly dispersed MnO_x species as amorphous phase over the two catalysts. The high concentration and high dispersion of Mn active species with amorphous phase on the surface were also verified for a superior SCR activity.^{44–46}

The surface chemical states of the catalysts were also examined and the results were listed in Table 2 and Fig. 4. The results showed that the surface concentrations of Mn species decreased with the increase of the chemical etching time. This could be attributed to the enhanced surface permeability of the support *via* chemical etching, which enabled more Mn species into the inside of the spherical structures.

The XPS spectra of Mn 2p_{3/2} in Fig. 4(a) clearly showed the Mn 2p_{3/2} peaks at about 642.0 eV.²⁵ The peak could be separated into three overlapped peaks of Mn²⁺, Mn³⁺ and Mn⁴⁺, respectively. The relative ratio of Mn⁴⁺ *via* deconvolution over the catalysts was summarized in Table 2. The Mn⁴⁺ content over Mn-SiO₂@TiO₂-2.5 catalyst is the highest among the other catalysts, which could be attributed to the high dispersion of

Mn species on the catalyst. According to previous report, the redox process of Mn⁴⁺ species was of utter importance in low-temperature SCR with NH₃.²⁶ High Mn⁴⁺ content could promote the oxidation process of NO to NO₂ and facilitate the “fast SCR” reaction, and thus enhance the low-temperature catalyst activity.⁴⁷ The surface contents of Mn⁴⁺ species on Mn/SiO₂ and Mn-SiO₂@TiO₂-1.5 catalyst are 39.96% and 26.22%, respectively, which is much lower than the other catalysts.

The O 1s XPS spectra of the catalysts were presented in Fig. 4(b), which could be separated into two peaks after a peak-fitting deconvolution. The peak at lower binding energy of 530.0 eV could be attributed to the lattice oxygen species O_α (Ti–O), while the peak at higher binding energy of 533–533.5 eV could be assigned to Si–O and chemisorbed oxygen O_β (mainly O⁻ or O₂²⁻ belonging to defect-oxide or hydroxyl-like group).^{48–50} Because of the high mobility, it is evident that the chemisorbed oxygen species are more active than the lattice oxygen species, suggesting the high amount of chemisorbed oxygen species is in favour of the oxidation of NO to NO₂ and the subsequent “fast SCR” reaction.⁵¹ However, Fig. 4(b) also showed the peak of O_β overlapped with the peak of Si–O bond in Mn/SiO₂, Mn-SiO₂@TiO₂-1.5 and Mn-SiO₂@TiO₂-2.5 samples. Although the trend of change in chemisorbed oxygen species could be observed in the XPS spectra, the XPS analysis results are still not adequate to determine the quantitative analysis of the chemisorbed oxygen species, further O₂-TPD analysis was needed to confirm the concentration of O_β over the catalysts.

3.2 O₂-TPD of the catalysts

O₂-TPD is an effective way to analyse the mobility and quantity of oxygen species, and the results of the oxygen desorption behaviour of the catalysts were shown in Fig. 5. At desorption temperature below 200 °C, the oxygen adsorption peaks could

Table 2 Chemical states of the Mn-based nano-cup catalysts

Samples	Mn (%)	O (%)	Mn ⁴⁺ (%)	Si–O + O _β /(O _α + O _β) (%)	Mn ⁴⁺ (%)
Mn/SiO ₂	5.03	66.77	39.96	87.32	2.00
Mn-SiO ₂ @TiO ₂	10.8	65.58	51.57	39.26	5.56
Mn-SiO ₂ @TiO ₂ -1.5	6.85	66.88	26.22	54.97	1.80
Mn-SiO ₂ @TiO ₂ -2.5	6.52	65.85	60.64	61.38	3.97
Mn-SiO ₂ @TiO ₂ -3	5.46	66.91	50.90	51.43	2.78



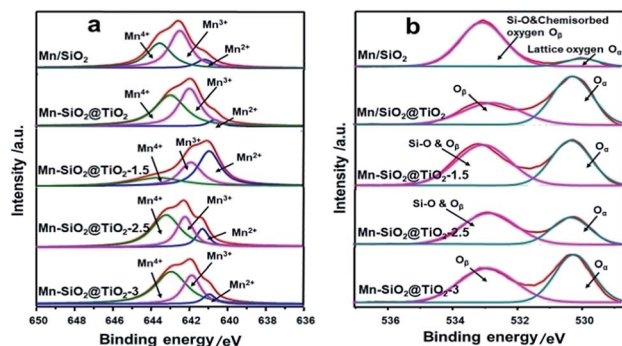


Fig. 4 (a) Mn $2p_{3/2}$ and (b) O $1s$ XPS spectra of the Mn-based nano-cup catalysts.

be observed on the Mn-SiO₂@TiO₂-1.5, Mn-SiO₂@TiO₂-2.5 and Mn-SiO₂@TiO₂-3 samples, while no significant desorption peaks on the Mn/SiO₂ and Mn-SiO₂@TiO₂ catalysts. This low-temperature desorption peaks may correspond to the physically adsorbed oxygen or weakly chemically adsorbed oxygen species.⁵² With the increase of desorption temperature, all samples showed oxygen desorption. The strong peak centred at around 500 °C was observed on all the samples, which could be assigned to strongly chemically absorbed O₂²⁻ or O⁻ species. These oxygen species are derived from the interaction of MnO_x and O₂. For the Mn-SiO₂@TiO₂-2.5 sample, an extra strong peak at around 590 °C suggested the strong interaction between the Mn and Ti species. Moreover, the strongly chemically absorbed oxygen peak at 500 °C of the Mn-SiO₂@TiO₂-2.5 sample was much higher and sharp than other catalysts, indicating the excellent oxygen adsorption capacity, which may lead to a favourable catalytic SCR reaction.⁵³

3.3 H₂-TPR of the catalysts

In order to analyse the redox behaviour of the catalysts, H₂-TPR was conducted and the results were presented in Fig. 6. For the Mn/SiO₂ and Mn-SiO₂@TiO₂ samples, the two strong reduction peaks at around 295 °C and 400 °C could be assigned to the reduction of MnO₂/Mn₂O₃ to Mn₃O₄ and the reduction of Mn₃O₄ to MnO, respectively.^{1,37} Consequently, the results of

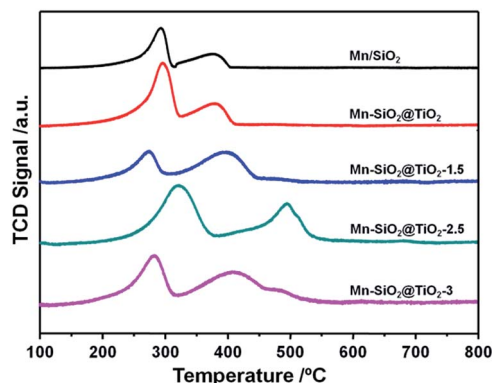


Fig. 6 H₂-TPR profiles of the Mn-based nano-cup catalysts.

TPR analysis agree well with that of XPS results. It is noticeable that the two reduction peaks in the profile of Mn-SiO₂@TiO₂-2.5 sample moved to a higher temperature. The decrease of reducibility over Mn-SiO₂@TiO₂-2.5 sample may be ascribed to a much strong interaction of Mn and Ti and good dispersion of surface active species over the catalyst, which will lead to a high stable SCR reaction. And the enhancing interaction of Mn and Ti over this sample could be explained by more Mn species entering into the bulk facet of Mn-SiO₂@TiO₂-2.5 rather than the surface facet of other catalysts. Moreover, the broader and larger reduction peak of Mn-SiO₂@TiO₂-2.5 sample than other samples suggested the higher oxygen storage ability and higher Mn⁴⁺ content. On the other hand, the Mn-SiO₂@TiO₂-1.5 sample showed lower reduction peak areas and therefore, only presented inferior SCR performance, especially in the lower temperature range. The H₂-TPR results are well in consistent with the O₂-TPD and activity results.

3.4 NH₃-TPD of the catalysts

The adsorption of NH₃ species was regarded as a key step in NH₃-SCR reaction, which greatly relies on the surface acidity of the catalysts.⁵⁴ Therefore, the surface acidity of the catalysts were analysed *via* NH₃-TPD, and the results were shown in Fig. 7. There were three main peaks over the Mn-SiO₂@TiO₂

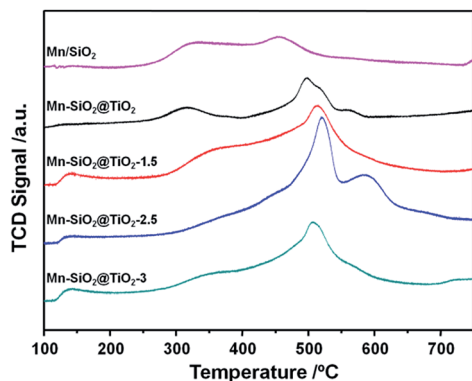


Fig. 5 O₂-TPD profiles of the Mn-based nano-cup catalysts.

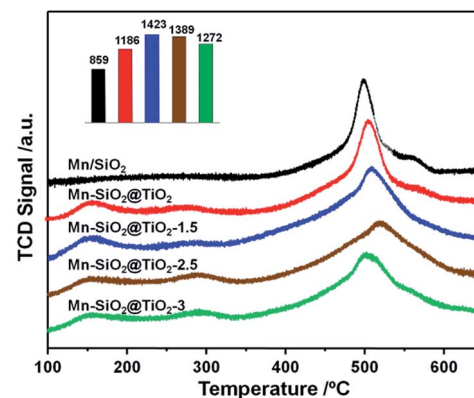


Fig. 7 NH₃-TPD profiles of the Mn-based nano-cup catalysts.



catalysts except for the Mn/SiO₂ sample. The first peak centred at around 150 °C could be assigned to desorption of physical adsorption NH₃ and some NH₄⁺ on the weak Brønsted acid sites. The second peak located at around 280 °C could be assigned to NH₄⁺ on the strong Brønsted acid sites. And the third strong peak was a broad NH₃ desorption peak from 350–650 °C, which represents the coordinated NH₃ species strongly adsorbed onto the Lewis acid sites.⁵⁵ The calculated areas of Lewis acid sites for Mn–SiO₂@TiO₂-1.5, Mn–SiO₂@TiO₂-2.5 and Mn–SiO₂@TiO₂-3 catalysts were 1423, 1389 and 1272, respectively, suggesting the surface acidity of these three samples were much higher than that of the Mn/SiO₂ and Mn–SiO₂@TiO₂ catalysts. The calculated areas of the peaks decreased gradually with the increase of the NaOH etching time, which makes sense since the alkaline NaOH would influence the surface acidity.

3.5 The catalytic activities and stabilities

The catalyst performance of the NO conversion and the N₂ selectivity as the function of reaction temperature were presented in Fig. 8. The catalytic activity of Mn–SiO₂@TiO₂-1.5 and Mn/SiO₂ catalysts were very low in the temperature range of 80–180 °C compared with the other three catalysts, which also showed distinct declination of NO_x conversion above 200 °C. Nevertheless, the Mn–SiO₂@TiO₂, Mn–SiO₂@TiO₂-2.5 and Mn–SiO₂@TiO₂-3 catalysts showed significant NO conversion (>80%) when the temperature at 140 °C and exhibited excellent activity in the temperature range of 140–240 °C. The Mn–SiO₂@TiO₂-2.5 sample achieved NO conversion of 45% at 80 °C and 100% in a wide operation temperature from 150 to 240 °C at the GHSV of 30 000 h^{−1}. However, the NO conversion of the Mn–SiO₂@TiO₂-3 catalyst showed much lower than that of Mn–SiO₂@TiO₂-2.5 catalyst in the low temperature (e.g., <160 °C).

The N₂ selectivities over the catalysts were illustrated in Fig. 8(b). It is obvious that the N₂ selectivity over Mn/SiO₂ catalyst dropped sharply during the whole temperature range due to the unselective catalytic oxidation of NH₃ on Mn/SiO₂ sample.⁵⁶ The N₂ selectivity of Mn–SiO₂@TiO₂, Mn–SiO₂@TiO₂-1.5 and Mn–SiO₂@TiO₂-3 samples dropped to around 80% at temperature of 180 °C. However, for the Mn–SiO₂@TiO₂-2.5

catalyst, the high N₂ selectivity (above 90%) was obtained during the whole operation temperature range indicated that the product of SCR reaction is in favour of N₂ and not N₂O over the Mn–SiO₂@TiO₂-2.5 catalyst.

From the characterizations (such as XRD, XPS, O₂/NH₃-TPD and H₂-TPR) above, the Mn–SiO₂@TiO₂ nano-cup catalyst was demonstrated with a large specific area, highly dispersed MnO_x as amorphous phase and high content of surface acidity. These properties are crucial for the SCR reaction. In addition, the Mn–SiO₂/TiO₂ nano-cup catalyst possesses high concentration of Mn⁴⁺ species and oxygen vacancy, which facilitate the activation of NH₃ and oxygen chemisorption of NO, and thus enhanced the low-temperature selective catalytic reduction of NO with NH₃.

To testify the stability of Mn-based nano-cup catalysts, the long-term stability test of the SCR reaction were performed over Mn–SiO₂@TiO₂-2.5 catalyst and the results were illustrated in Fig. 9. When the NO conversion reached up to 100% after reaction for 3 h over the Mn–SiO₂@TiO₂-2.5 catalyst, it showed an excellent SCR stability with a NO conversion stable at a value of 100% during the next 120 h test. The high stability could be attributed to the high dispersion of the MnO₂ active sites and the unique annulus structure between mesoporous TiO₂ layers and SiO₂ sphere for stabilizing the MnO₂ nanoparticles. Moreover, we added the characterizations of the 120 h-stability-tested Mn–SiO₂@TiO₂-2.5 sample using XRD, BET and SEM techniques, respectively. The BET surface of the used catalyst is *ca.* 64 m² g^{−1}, which showed a slight decrease compared with the fresh sample. The XRD results (Fig. S1†) showed a low intensity of MnO₂ in the used sample, indicating that MnO_x species still maintained its high dispersity and stability during the reaction process. Moreover, the SEM image (Fig. S2†) showed that the used catalyst could maintain the morphologies after the long-time reaction. In addition, the impacts of H₂O and SO₂ on the SCR activity of Mn–SiO₂@TiO₂-2.5 sample have also been investigated and the results were summarized in Fig. S3.† The results showed that the NO conversion over the Mn–SiO₂@TiO₂-2.5 decreased from the initial 100% to 90% with the introduction of 5 vol% H₂O. However the performance could be recovered after switching off H₂O. With the addition of SO₂

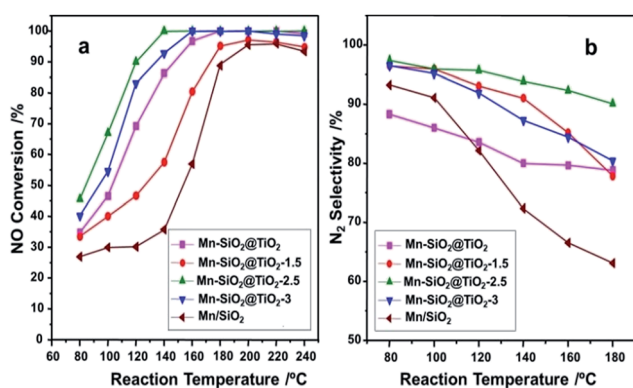


Fig. 8 The NO_x conversion (a), and N₂ selectivity (b) of the Mn-based nano-cup catalysts. Reaction conditions: [NO] = [NH₃] = 1000 ppm, [O₂] = 5%, balance N₂, GHSV = 30 000 h^{−1}.

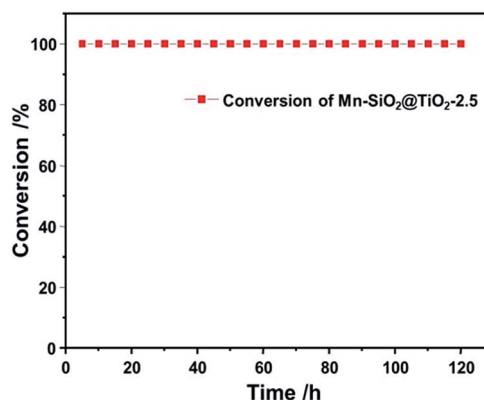


Fig. 9 Stability test profile of the Mn–SiO₂@TiO₂-2.5 catalyst.



(200 ppm) for 4 h, the NO conversion declined to about 42% and could not be recovered after switching off SO₂. Since the SO₃ from the oxidation of SO₂ reacts with NH₃ to form NH₄HSO₄ and (NH₄)₂SO₄, they could physically block the active sites and result in the drop of SCR activity. Therefore, the SO₂ resistance of manganese-based catalyst at low temperature still needed the further improvement.

3.6 The role of MnO₂ species and acidic sites of Mn-SiO₂/TiO₂ nano-cup catalyst for SCR reaction

On the basis of the characterizations and the catalytic performance of the Mn-SiO₂@TiO₂ catalysts, both the MnO_x species and surface acid sites are playing an essential role in the low-temperature selective catalytic reduction of NO with NH₃. Therefore, we proposed a synergism between MnO₂ and acid sites over Mn-SiO₂@TiO₂ nano-cups for low-Temperature SCR reaction and the mechanism was illustrated in Fig. 10.

At first, the NH₃ molecule was absorbed onto the Lewis acid center and the oxygen atoms of the MnO₂ sites to form aminoxy groups, while the NO absorbs onto the surface oxygen vacancies as nitrosyls. Second, the absorbed NO would be oxidized to gas-phase NO₂ in the presence of gas-phase oxygen and oxygen vacancies were recovered.^{57,58} The SCR reaction happened between aminoxy groups and gas-phase NO₂ to produce N₂ and H₂O *via* the surface dehydroxylations and re-oxidation of oxygen vacancies. At the same time, NH₃ molecule could be adsorbed onto the neighboring Brønsted acid sites on the SiO₂@TiO₂ support. The adsorbed NH₃ would react with NO₂ to form an active complex. This step may include NO oxidation to NO₂ or diffusion of NO₂ to adsorbed NH₃ if significant gas-phase NH₃ is present. The oxidation of NO to NO₂ plays an important role in NH₃-SCR reaction through “fast SCR” pathway: $\text{NO} + \text{NO}_2 + 2\text{NH}_3 \rightarrow 2\text{N}_2 + 3\text{H}_2\text{O}$.⁵⁹ The NO oxidation of Mn-SiO₂@TiO₂-2.5 was tested and demonstrated in Fig. S5† and NO-TPD analysis was also performed to investigate the adsorption behavior of NO over the five catalyst samples and the results are shown in Fig. S6.† The formed active complex will react rapidly with NO or NO₂ to form N₂/N₂O and H₂O. Then the catalyst surface was recovered and the SCR reaction process cycles. It is possible that the interactions with other NH₃ molecules will enhance the decomposition process and facilitates the new SCR cycles. From the proposed synergistic mechanism, the superior NO conversion and N₂ selectivity over the Mn-SiO₂@TiO₂-2.5 catalyst could be attributed to its higher concentration of Mn⁴⁺ and Lewis acid sites, as well as the

higher oxygen storage ability. The inferior N₂ selectivity of Mn/SiO₂ sample might result from the subsequent formation of surface nitrate groups since the NO₂ could react rapidly with the active complex to generate N₂O.

4. Conclusions

A novel Mn-SiO₂@TiO₂ nano-cup catalyst was synthesized *via* the coating of the mesoporous TiO₂ layers on SiO₂ sphere and subsequent inlay of MnO₂ nanoparticles in the narrow annulus. The Mn-SiO₂@TiO₂-2.5 catalyst exhibited superior activity and stability for low-temperature selective catalytic reduction of NO with NH₃, with a NO conversion of ~100%, N₂ selectivity above 90% at the temperature ~140 °C, and a stable performance during the 120 h stability test. The characterizations results indicated that this nano-cup structure of the Mn-SiO₂@TiO₂-2.5 catalyst possesses high concentration and dispersion of Mn⁴⁺ active species, strong chemisorbed O⁻ or O₂²⁻ species and highly stable MnO_x active components over the annular structures of TiO₂ shell and SiO₂ sphere, and thus are favourable to the low-temperature selective catalytic reduction of NO with NH₃.

Conflicts of interest

There are no conflicts to declare.

Acknowledgements

The authors are grateful for the support from the Natural Science Foundation of China (21236004, 21576169).

Notes and references

- 1 R. Guo, M. Li, P. Sun, S. Liu, S. Wang, W. Pan, S. Liu, J. Liu and X. Sun, *RSC Adv.*, 2017, 7, 19912–19923.
- 2 R. Guo, S. Wang, W. Pan, M. Li, P. Sun, S. Liu, X. Sun, S. Liu and J. Liu, *J. Phys. Chem. C*, 2017, **121**, 7881–7891.
- 3 S. Andreoli, F. A. Deorsola, C. Galletti and R. Pirone, *Chem. Eng. J.*, 2015, **278**, 174–182.
- 4 R. Guo, W. Pan, X. Zhang, H. Xu, Q. Jin, C. Ding and S. Guo, *Sep. Sci. Technol.*, 2013, **48**, 2871–2875.
- 5 T. Zhang, J. Liu, D. Wang, Z. Zhao, Y. Wei, K. Cheng, G. Jiang and A. Duan, *Appl. Catal., B*, 2014, **148**, 520–531.
- 6 L. Zhu, Z. Zhong, H. Yang and C. Wang, *Water, Air, Soil Pollut.*, 2016, **227**, 476.
- 7 J. Ding, J. Lin, J. Xiao, Y. Zhang, Q. Zhong, S. Zhang, L. Guo and M. Fan, *J. Alloys Compd.*, 2016, **665**, 411–417.
- 8 J. Liu, X. Li, Q. Zhao, J. Ke, H. Xiao, X. Lv, S. Liu, M. Tade and S. Wang, *Appl. Catal., B*, 2017, **200**, 297–308.
- 9 R. Guo, Y. Zhou, W. Pan, J. Hong, W. Zhen, Q. Jin, C. Ding and S. Guo, *J. Ind. Eng. Chem.*, 2013, **19**, 2022–2025.
- 10 C. Liu, L. Chen, J. Li, L. Ma, H. Arandiyana, Y. Du, J. Xu and J. Hao, *Environ. Sci. Technol.*, 2012, **46**, 6182–6189.
- 11 L. Zhang, D. Zhang, J. Zhang, S. Cai, C. Fang, L. Huang, H. Li, R. Gao and L. Shi, *Nanoscale*, 2013, **5**, 9821–9829.
- 12 P. Wang, Q. Wang, X. Ma, R. Guo and W. Pan, *Catal. Commun.*, 2015, **71**, 84–87.

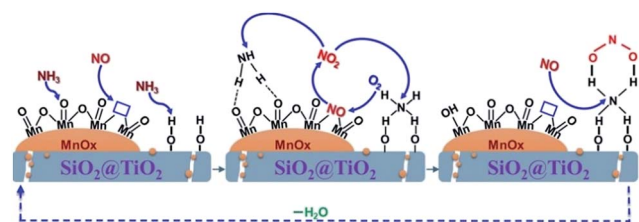


Fig. 10 The proposed synergism between MnO₂ and acid sites over Mn-SiO₂@TiO₂ nano-cups for low-Temperature SCR reaction.



- 13 X. Xie, J. Lu, E. Hums, Q. Huang and Z. Lu, *Energy Fuels*, 2015, **29**, 3890–3896.
- 14 J. Yu, F. Guo, Y. Wang, J. Zhu, Y. Liu, F. Su, S. Gao and G. Xu, *Appl. Catal., B*, 2010, **95**, 160–168.
- 15 P. R. Ettireddy, N. Ettireddy, S. Mamedov, P. Boolchand and P. G. Smirniotis, *Appl. Catal., B*, 2007, **76**, 123–134.
- 16 B. Thirupathi and P. G. Smirniotis, *Appl. Catal., B*, 2011, **110**, 195–206.
- 17 S. Cai, J. Liu, K. Zha, H. Li, L. Shi and D. Zhang, *Nanoscale*, 2017, **9**, 5648–5657.
- 18 S. Xiong, Y. Liao, X. Xiao, H. Dang and S. Yang, *Catal. Sci. Technol.*, 2015, **5**, 2132–2140.
- 19 L. Huang, X. Hu, S. Yuan, H. Li, T. Yan, L. Shi and D. Zhang, *Appl. Catal., B*, 2017, **203**, 778–788.
- 20 Y. J. Kim, H. J. Kwon, I. S. Nam, J. W. Choung, J. K. Kil, H. J. Kim, M. S. Cha and G. K. Yeo, *Catal. Today*, 2010, **151**, 244–250.
- 21 J. Chen, Y. Zheng, W. Cai, H. Zou, W. Zheng, Y. Zhang, X. Chen and B. Fu, *Micro Nano Lett.*, 2017, **12**, 6–10.
- 22 G. Qi and R. Yang, *Appl. Catal., B*, 2003, **44**, 217–225.
- 23 H. Jiang, C. Wang, H. Wang and M. Zhang, *Mater. Lett.*, 2016, **168**, 17–19.
- 24 D. K. Pappas, T. Boningari, P. Boolchand and P. G. Smirniotis, *J. Catal.*, 2016, **334**, 1–13.
- 25 M. Kang, E. D. Park, J. M. Kim and J. E. Yie, *Appl. Catal., A*, 2007, **327**, 261–269.
- 26 C. Fang, D. Zhang, S. Cai, L. Zhang, L. Huang, H. Li, P. Maitarad, L. Shi, R. Gao and J. Zhang, *Nanoscale*, 2013, **5**, 9199–9207.
- 27 D. A. Pena, B. S. Uphade and P. G. Smirniotis, *J. Catal.*, 2004, **221**, 421–431.
- 28 Y. Chen, J. Wang, Z. Yan, L. Liu, Z. Zhang and X. Wang, *Catal. Sci. Technol.*, 2015, **5**, 2251–2259.
- 29 S. Cai, H. Hu, H. Li, L. Shi and D. Zhang, *Nanoscale*, 2016, **8**, 3588–3598.
- 30 H. Hu, S. Cai, H. Li, L. Huang, L. Shi and D. Zhang, *ACS Catal.*, 2015, **5**, 6069–6077.
- 31 L. Zhang, L. Shi, L. Huang, J. Zhang, R. Gao and D. Zhang, *ACS Catal.*, 2014, **4**, 1753–1763.
- 32 T. Boningari and P. G. Smirniotis, *Curr. Opin. Chem. Eng.*, 2016, **13**, 133–141.
- 33 N. Yang, R. Guo, Q. Wang, W. Pan, Q. Chen, C. Lu and S. Wang, *RSC Adv.*, 2016, **6**, 11226–11232.
- 34 P. R. Ettireddy, N. Ettireddy, T. Boningari, R. Pardemann and P. G. Smirniotis, *J. Catal.*, 2012, **292**, 53–63.
- 35 K. Lv, Q. Xiang and J. Yu, *Appl. Catal., B*, 2011, **104**, 275–281.
- 36 J. Yu, S. Liu and H. Yu, *J. Catal.*, 2007, **249**, 59–66.
- 37 S. Deng, T. Meng, B. Xu, F. Gao, Y. Ding, L. Yu and Y. Fan, *ACS Catal.*, 2016, **6**, 5807–5815.
- 38 M. Fu, C. Li, P. Lu, L. Qu, M. Zhang, Y. Zhou, M. Yu and Y. Fang, *Catal. Sci. Technol.*, 2014, **4**, 14–25.
- 39 G. Li, J. Liu, J. Lan, G. Li, Q. Chen and G. Jiang, *CrystEngComm*, 2014, **16**, 10547–10552.
- 40 Y. Yang, G. Wang, Q. Deng, H. Wang, Y. Zhang, D. H. L. Ng and H. Zhao, *RSC Adv.*, 2014, **4**, 34577–34583.
- 41 C. Hu, X. Zhang, W. Li, Y. Yan, G. Xi, H. Yang, J. Li and H. Bai, *J. Mater. Chem. A*, 2014, **2**, 2040–2043.
- 42 S. Yang, J. Li, C. Wang, J. Chen, L. Ma, H. Chang, L. Chen, Y. Peng and N. Yan, *Appl. Catal., B*, 2012, **117**, 73–80.
- 43 S. Ali, L. Chen, F. Yuan, R. Li, T. Zhang, S. u. H. Bakhtiar, X. Leng, X. Niu and Y. Zhu, *Appl. Catal., B*, 2017, **210**, 223–234.
- 44 G. S. Qi and R. T. Yang, *J. Catal.*, 2003, **217**, 434–441.
- 45 W. S. Kijlstra, D. S. Brands, E. K. Poels and A. Blik, *J. Catal.*, 1997, **171**, 208–218.
- 46 H. Y. Huang and R. T. Yang, *Langmuir*, 2001, **17**, 4997–5003.
- 47 A. Grossale, I. Nova, E. Tronconi, D. Chatterjee and M. Weibel, *J. Catal.*, 2008, **256**, 312–322.
- 48 J. C. Dupin, D. Gonbeau, P. Vinatier and A. Levasseur, *Phys. Chem. Chem. Phys.*, 2000, **2**, 1319–1324.
- 49 P. Yang, Z. Quan, Z. Hou, C. Li, X. Kang, Z. Cheng and J. Lin, *Biomaterials*, 2009, **30**, 4786–4795.
- 50 L. Ma, J. Li, R. Ke and L. Fu, *J. Phys. Chem. C*, 2011, **115**, 7603–7612.
- 51 Z. Wu, R. Jin, Y. Liu and H. Wang, *Catal. Commun.*, 2008, **9**, 2217–2220.
- 52 G. Qi and W. Li, *Catal. Today*, 2015, **258**, 205–213.
- 53 P. Li, C. He, J. Cheng, C. Y. Ma, B. J. Dou and Z. P. Hao, *Appl. Catal., B*, 2011, **101**, 570–579.
- 54 N. Y. Topsoe, *Science*, 1994, **265**, 1217–1219.
- 55 N. Yang, R. Guo, W. Pan, Q. Chen, Q. Wang and C. Lu, *Fuel*, 2016, **169**, 87–92.
- 56 J. Liu, J. Liu, Z. Zhao, Y. Wei, W. Song, J. Li and X. Zhang, *Ind. Eng. Chem. Res.*, 2017, **56**, 5833–5842.
- 57 W. Tian, H. Yang, X. Fan and X. Zhang, *J. Hazard. Mater.*, 2011, **188**, 105–109.
- 58 X. Fan, F. Qiu, H. Yang, W. Tian, T. Hou and X. Zhang, *Catal. Commun.*, 2011, **12**, 1298–1301.
- 59 Q. Li, H. S. Yang, F. M. Qiu and X. B. Zhang, *J. Hazard. Mater.*, 2011, **192**, 915–921.

